Supporting Information

Trichet et al. 10.1073/pnas.1117810109

SI Text

Cell Culture. The cells were deposited on μFSA 3 to 6 h before microscopy experiments. Cells on micropillar substrates were fixed for 10 min at room temperature using 3% formaldehyde, 4% sucrose in PBS, rinsed in PBS, and permeabilized for 5 min with 0.5% Triton X-100 in PBS, after which they were blocked for 1 h with 3% BSA in PBS and rinsed again in PBS. The actin cytoskeleton was stained with Alexa 633 phalloidin at 1/1,000 dilution.

Preparation and Calibration of Microstructured Polydimethylsiloxane (PDMS) Substrates. We used dimensionally calibrated macroscopic cylinders of this material and measured their compression under a fixed normal strain to determine the Young's modulus, E, of the PDMS. As E depends on the PDMS cure time, we used a consistent cure time of 15 h ± 2 h at 65 °C. E strongly depends on the fraction of the crosslinker added, which we varied from 3.3–10% corresponding to values ranging from $E = 0.3$ to 1.8 MPa. Above 5% crosslinker, we obtained a linear relationship between the fraction of crosslinker and the value of E. By performing scanning electron microscopy (SEM) observations, we measured the dimensions of the pillars. We used pillars with a diameter of 2 μm and a center-to-center distance of 4 μm. For the durotaxis experiment, the substrates were composed of consecutive arrays of micropillars of diameters 1 and 2 μm while the surface density of the micropillars was kept constant.

Only the top of the pillars was coated with fluorescently labeled fibronectin (Cy3; Amersham Biosciences). To achieve this coating, a stamp of flat PDMS was inked with a PBS solution containing 50 μg/mL of fibronectin and 5 μg/mL of labeled Cy3 fibronectin. The stamps were then dried and placed against the microforce sensor array (μFSA) for 10 min. Then we treated the substrates with pluronics (F127) for 1 h and rinsed with PBS 1× to prevent cell adhesion along the pillars.

Time-Lapse Video-Microscopy. Time-lapse images of cells on pillars were acquired using an Olympus BX51 upright microscope, equipped with an incubator maintaining the temperature at 37 °C.

For the durotaxis experiments, time-lapse sequences were acquired over 16 h using a frame delay of 5 min on the inverted microscope. Images were taken using an Olympus 20× air objective lens (N.A. 0.40). Using an automated stage, driven by Metamorph (Marzhauser), we observed different areas during the same experiment ($40 < n_{\text{cells}} < 80$).

For the force measurements, time-lapse sequences were acquired over 30 min to 1 h using a frame delay of 30 s to 3 min on the upright microscope. The cells were observed with an Olympus 60× water immersion objective lens (N.A. 0.9). Pillars were imaged with the aid of the signal from the fluorescent fibronectin coating their tops. Both images (pillars and focal adhesions) were taken at each time point using the automated filter turret control, driven by Metamorph.

Image Analysis, Focal Adhesion Characterization, and Force Traction Measurements. We analyzed the time-lapse images using ImageJ software (National Institutes of Health). We determined the position of the adhesions for each picture and substracted the background. We then used the smooth filter, which replaced each pixel with the average of its 3 × 3 neighborhood. All focal adhesions were thresholded and their areas over time were determined using the Particle Tracker plugin.

We used a homemade multiparticle tracking routine to detect micropillar positions for each image from the fluorescent signal emitted by the labeled fibronectin coating the top of the pillars. The contrast was high enough to determine the pillar position with a resolution of approximately 20–30 nm. We then calculated the displacement of each pillar by comparing the positions with the undeflected positions. The applied forces were deduced by multiplying the displacements by the spring constant of the pillars.

To relate the FA area and the force, we measured the corresponding FA area and pillar displacement. All data averaged measurements done on at least 15 different focal adhesions (or pillars) in at least five different cells.

Statistics collected on the focal adhesion area distribution involved analysis of 70 different focal adhesions in at least six different cells, placed on μFSAs of different rigidities.

Durotaxis analysis was performed by counting the preferential orientation of cells after touching the boundary between the two different parts of the substrate. Cells coming from the soft part or from the stiff part were considered independently. Each statistic refers to the analysis of 40 to 80 different cells. Statistics on microcontact-printing experiments were collected on 27 cells coming from the side with 2-μm fibronectin-patches and 29 cells coming from the side with 1-μm patches, respectively.

Scanning Electron Microscopy. Cells were cultured on a μFSA after their previous resuspension, fixed with 4% paraformaldehyde in PBS for 1 h and then further rinsed three times with PBS buffer. Dehydration was performed by rinsing the samples through graded ethanol/water mixtures (50, 70, 80, 90, and finally 100%, 10 min per step). Ethanol was slowly exchanged successively by amyl acetate and liquid CO_2. Finally, samples were dried using the critical point method and then coated by sputtering with a thin layer of gold.

Theoretical Modeling of Cell Mechanosensitivity. Focal adhesions (FAs) play an important role in mechanotransduction, as shown by the reported dependence of their size on the sustained force. The usual generic mechanism invoked to account for this mechanosensitivity is that a force applied on an FA induces an elastic deformation of the contact that triggers conformational and organizational changes (such as unfolding) of some of its constitutive proteins, which in turn can enhance binding with new proteins and enable the growth of the contact. Initially, we give theoretical arguments based on a simple phenomenological model inspired by Nicolas et al. (1), which shows that FAs can act as mechanosensors and display an adaptive response to the local mechanical properties (elastic modulus) of their immediate environment, namely the extracellular matrix (ECM). We next show that this mechanosensitivity, based on mechanisms at the molecular scale, is only local, and cannot therefore explain the response to large-scale mechanical properties, such as the rigidity of pillar, as reported here. This failure of the simple model supports the existence of another mechanosensing mechanism, which we suggest could be mediated by the deformation of cytoskeletal structures such as stress fibers. Here our purpose is to provide theoretical arguments to support the existence of such a large-scale mechanosensing mechanism rather than to design an explicit model with specific functional forms.

Local mechanosensitivity. We first consider an FA bound to a flat substrate. We model the substrate and its coating of ECM molecules (such as fibronectin) as a linear elastomer of Young's mod-

ulus E_s. The FA plaque, of area S_{FA} and thickness d, is modeled as a homogeneous linear elastomer of Young's modulus E_{FA} and Poisson ratio ν_{FA}. A longitudinal and homogeneous stress $\sigma = F/S_{FA}$ is applied along the upper surface of the FA (direction x). We denote by u_s the deformation field (constant in a first approximation) along x at the substrate/FA interface, and u_{FA} the deformation field of the upper surface of the FA. Given the timescales involved (mins) in the mechanical response of the cell, we assume the forces are balanced and obtain, as follows:

$$F = \sigma A = g_{FA} u_{FA} S_{FA} = k_s u_s, \qquad \textbf{[S1]}$$

where $g_{FA} = E_{FA}/[2d(1+\nu_{FA})]$ and $k_s \propto E_s$. Following Nicolas et al. (1, 2), we first assume that the dynamics of S_{FA} is coupled to the deformation of the substrate u_s. This coupling can be written generically as

$$\frac{dS_{FA}}{dt} = f(u_s, S_{FA}), \qquad \textbf{[S2]}$$

where f is an increasing function of u_s which typically decreases for large S_{FA}, defining a steady state area $S_{FAss}(u_s)$ by $f(u_s, S_{FAss}) = 0$.

This phenomenological model accounts for the effect mentioned above that an elastic deformation of the substrate induces conformational changes of ECM molecules and makes new binding sites for FA proteins available. Typically, a linear dependence for small u_s can be expected. The explicit form of f depends on the microscopic modelling and will not be discussed here [Nicolas et al. (1)] for a possible functional form. In particular, this model shows that the kinetics of FA growth depends on the applied force (because $u_s = F/k_s$), as observed in experiments (3).

For the FA to function as an autonomous mechanosensor, the stress σ applied by the stress fiber on the FA has to be regulated by the FA itself, even if indirectly. This feedback can be generically written as follows:

$$\sigma = h[u_{FA}], \qquad \textbf{[S3]}$$

where the brackets means functional dependence. This constitutive equation determines the stress applied by the stress fiber thereby completing the set of equations, Eqs. **S1–S3**. As above, a hypothetical molecular basis of this feedback relies on the shear-induced conformational changes of FA proteins, which enhance actin polymerization on the FA plaque and therefore increase the stress. Note finally that refinements of this model can be added, for instance to account for shear stiffening of the substrate, by taking $g_{FA}(u_s, u_{FA})$.

The point that we make here is that the Eqs. **S1–S3** fully determine the unknowns S_{FA}, σ, u_s, u_{FA} as functions of E_s only as parameter of the environment of the FA. This set of equations defines very generally the local mechanosensitive response of the FA, already observed in previous studies (3). Here our purpose is to provide a generic outline; we therefore do not give explicit functional forms.

Large-scale mechanosensitivity. We now show that the mechanosensitivity effect that we report in this paper is not due only to the previously reported mechanism mediated by FAs, and that it requires a larger scale mechanism. We keep the same notations as in previous paragraph, except that now the substrate is not infinite, but elastically bound to a wall by a spring of stiffness k, accounting for the pillar elasticity. Note that k can be varied by tuning the geometric parameters of the pillars and keeping E_s constant.

We denote by x the displacement of the pillar along the force direction. All the equations in the previous paragraph still hold (in the shifted frame of the pillar surface, and assuming that the local deformation u_s is much smaller than the global displacement x), and mechanical equilibrium gives the extra equation $F = kx$ for the extra variable x. This equation is independent of Eqs. **S1–S3** above, which shows straightforwardly that if the feedback is mediated by the FA only as above, then S_{FA}, σ, u_s, u_{FA} will depend on E_s only and not on k, which can be varied independently of E_s through the geometric parameters of the pillar. However, our experimental findings are that the stress depends on k (Fig. 3*A*). We therefore conclude that extra feedback involving other structures than FAs must be involved. We suggest below that this feedback could be mediated by the cytoskeleton, and in particular by stress fibers pulling on the FAs. We therefore write instead of Eq. **S3**:

$$\sigma = h[x(t)]. \qquad \textbf{[S4]}$$

The system (Eq. **S1**, **S2**, **S4**) is now fully coupled, and generically the resulting stress will now depend on k, as observed experimentally. As a result, a large-scale mechanosensing mechanism realized by the coupling **[S4]** must exist.

Cytoskeleton-based mechanosensitivity. The coupling (Eq. **S4**) means that a deformation of the cytoskeleton (here a shortening of length x of a stress fiber) impacts on the active stress exerted by the cytoskeleton. On general grounds, such coupling can be justified in the framework of the theory of viscoelastic active gels (4). This theory states by symmetry arguments that in polar or nematic media driven out of equilibrium such as the cytoskeleton, there exists an active stress σ^a_{ij} (here due to actin/myosin interactions) proportional to the nematic tensor $Q_{ij} = \langle n_i n_j \rangle - \delta_{ij}/3$ and reads $\sigma^a_{ij} = \alpha Q_{ij}$ where α is a phenomenological coupling constant. Here n_i denotes the orientation vector of a single actin filament and the average is taken locally over a coarse-graining length scale. In the case of a quasi two-dimensional adhering cell, we obtain

$$Q_{\theta_0\theta_0} = \langle \cos 2(\theta\text{-}\theta_0) \rangle, \qquad \textbf{[S5]}$$

which quantifies the polarization along the direction θ_0, where θ denotes the angle of n with a reference axis. The scalar order parameter S is then defined as $S = Q_{\langle\theta\rangle\langle\theta\rangle}$, where $\langle\theta\rangle$ is the preferred direction of the system. Because imaging of single actin filaments is not accessible in our set-up, stress fibers can be used as a coarse-grained order parameter to evaluate Q_{ij}. In generic visco elastic nematic materials, the nematic tensor is in turn coupled to the strain U_{ij}. More qualitatively, this coupling means that a local deformation x induces a strain U_{ij} in the cytoskeleton and therefore a reorganization of the orientation Q_{ij} of the filaments, which in turn yields an active stress. This coupling between Q_{ij} and U_{ij} can be verified experimentally. We found that a strong dependency of the order parameter with the rigidity of the substrate. In the case of rigid substrate ($k = 100$ nN/μm) (small strain U_{ij}), the cells are polarized so that $\langle S \rangle \approx 0.8$ (Fig. 4*C*). On the contrary, in the case of a soft substrate ($k = 4$ nN/μm) (large strain U_{ij}), stress fibers showed no preferred direction, yielding $S \approx 0.19$ (Fig. 4*A*). At intermediate stiffness (≈40 nN/μm), we obtained $\langle S \rangle = 0.56$ (Fig. 4*B*).

In a first approximation, as in the model introduced in Zemel et al. (5), a linear coupling can be suggested of the form,

$$\sigma^a = -\gamma(U - U^0), \qquad \textbf{[S6]}$$

where U^0 is the initial contractile strain and γ is a fourth rank tensor (indexes have been dropped) which determines the active response of the cell to deformation. Such coupling was found compatible with observations of the response of stem cells to matrix stiffness in Zemel et al. (5).

Such a model can be made more explicit at the scale of a single stress fiber, which is a one-dimensional structure with well-de-

fined boundary conditions, because stress fibers end at focal adhesions. In this case Eq. **S6** can be rewritten as

$$\sigma^a = -\gamma(x - x^0). \quad \textbf{[S7]}$$

The force balance condition then yields $F = kx = \sigma^a S_{\mathrm{FA}}$ where S_{FA} denotes the area of the focal adhesion ending the stress fiber. We finally obtain

$$\sigma^a = \frac{k\gamma x^0}{k + \gamma S_{\mathrm{FA}}}, \quad \textbf{[S8]}$$

which can be fitted to experimental results of Fig. 3*B*. Additionally, we can obtain the force which reads, as follows:

$$F = \frac{k\gamma x^0 S_{\mathrm{FA}}}{k + \gamma S_{\mathrm{FA}}}. \quad \textbf{[S9]}$$

This functional form of the force as a function of substrate stiffness is compatible with the model introduced in Zemel et al. (5), which is also based on linear response. In the regime of small stiffness k, it yields to linear order $F \approx kx^0$, which corresponds to the experimental results of Fig. 2*C*. The parameter x^0, which can be fitted from the data to the value $x^0 \approx 800$ nm, can be interpreted as the typical shortening length of a stress fiber. For a typical stress fiber length of 10 μm, this result is compatible with observations (6) where a 5–15% shortening was obtained.

1. Nicolas A, Geiger B, Safran SA (2004) Cell mechanosensitivity controls the anisotropy of focal adhesions. *Proc Natl Acad Sci USA* 101:12520–12525.
2. Nicolas A, Safran SA (2006). Limitation of cell adhesion by the elasticity of the extracellular matrix. *Biophys J* 91:61–73.
3. Balaban NQ, et al. (2001) Force and focal adhesion assembly: A close relationship studied using elastic micropatterned substrates. *Nat Cell Biol* 3:466–472.
4. Kruse K, Joanny JF, Julicher F, Prost J, Sekimoto K (2005) Generic theory of active polar gels: A paradigm for cytoskeletal dynamics. *Eur Phys J E* 16:5–16.
5. Zemel A, Rehfeldt F, Brown AEX, Discher DE, Safran SA (2010) Optimal matrix rigidity for stress-fibre polarization in stem cells. *Nat Phys* 6:468–473.
6. Kreis TE, Birchmeier W (1980) Stress fiber sarcomeres of fibroblasts are contractile. *Cell* 22:555–561.

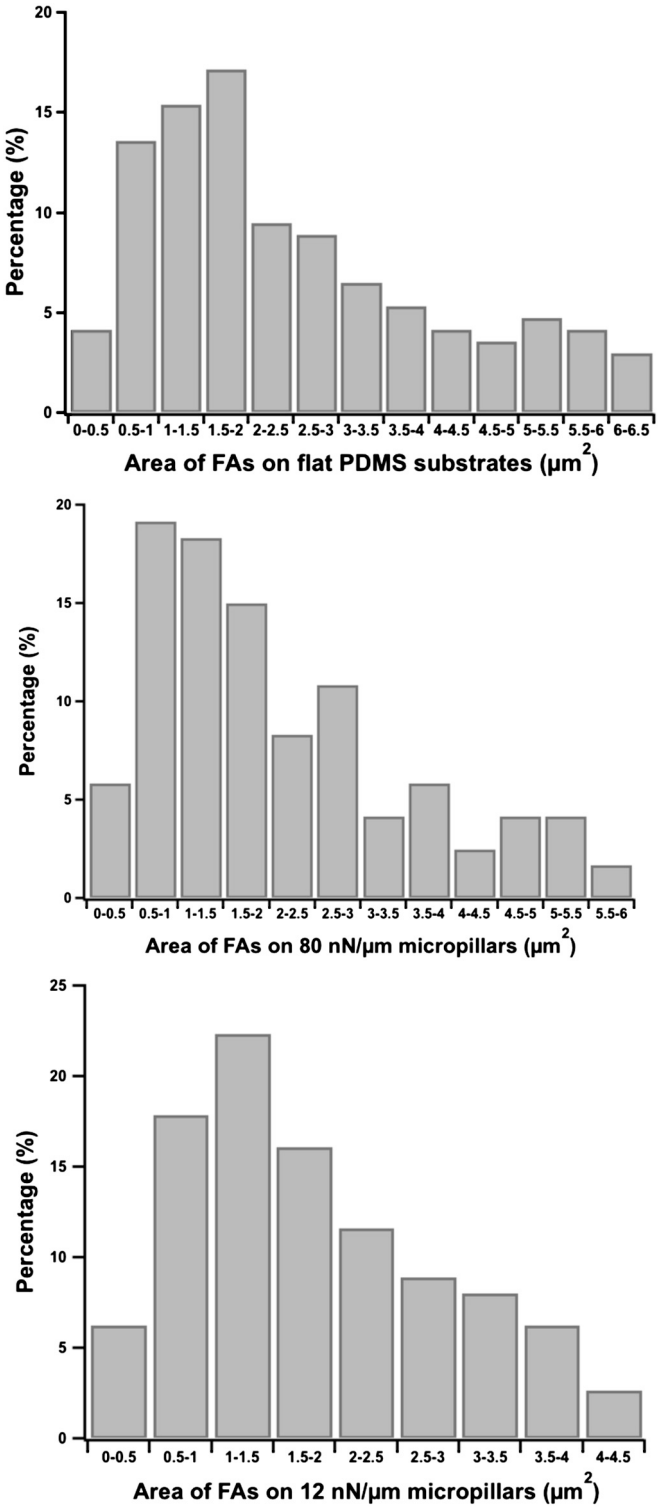

Fig. S1. Distribution of focal adhesions areas on micropillar substrates and flat PDMS substrates.

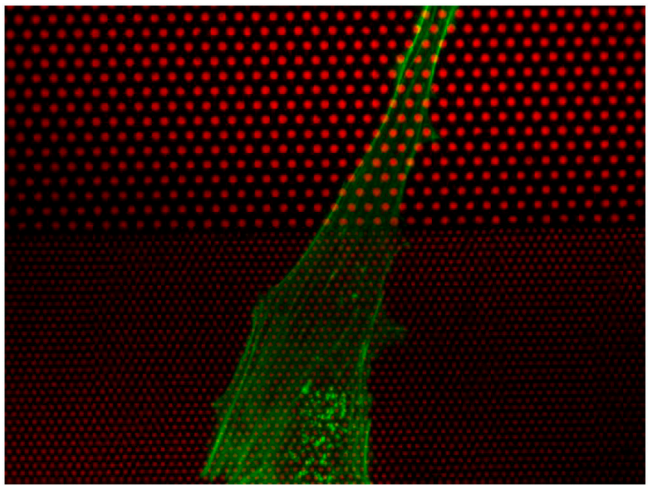

Fig. S2. Micropatterned substrates for durotaxis control experiment. Cell adhesion on glass micropatterned substrates at the boundary between 1- and 2-μm fibronectin patches (red). The density of fibronectin patches was kept constant between both sides of the substrates. Actin cytoskeleton is labeled in green.

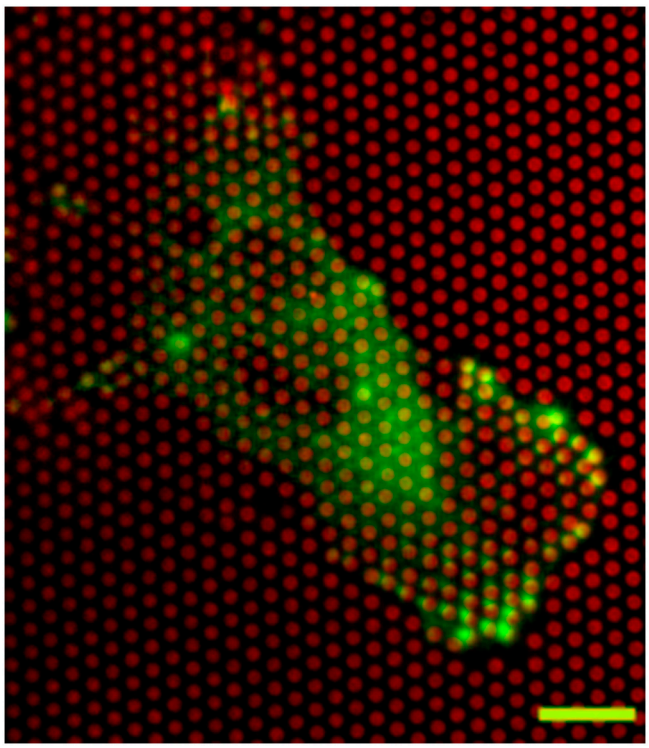

Movie S1. An example of the traction forces over time exerted by an REF52 cell expressing YFP-paxillin (green) on micropillars stamped with fluorescent fibronectin (red). (Scale bar, 10 μm.) The duration of the movie is 2 h.
Movie S1 (AVI)

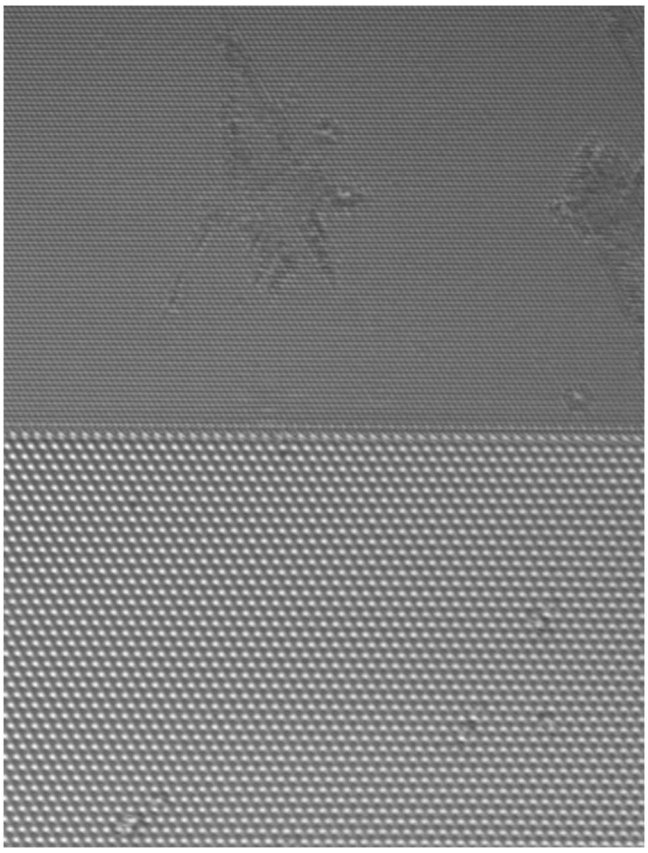

Movie S2. An example of the cell movements at the boundary between a stiff substrate ($K_s = 80$ nN/μm; pillar diameter = 2 μm) and a soft substrate ($k_s = 7$ nN/μm; pillar diameter = 1 μm). The cell first comes from the soft part of the substrate and transmigrates toward the stiff part with a perpendicular orientation with regards to the boundary.

Movie S2 (MOV)

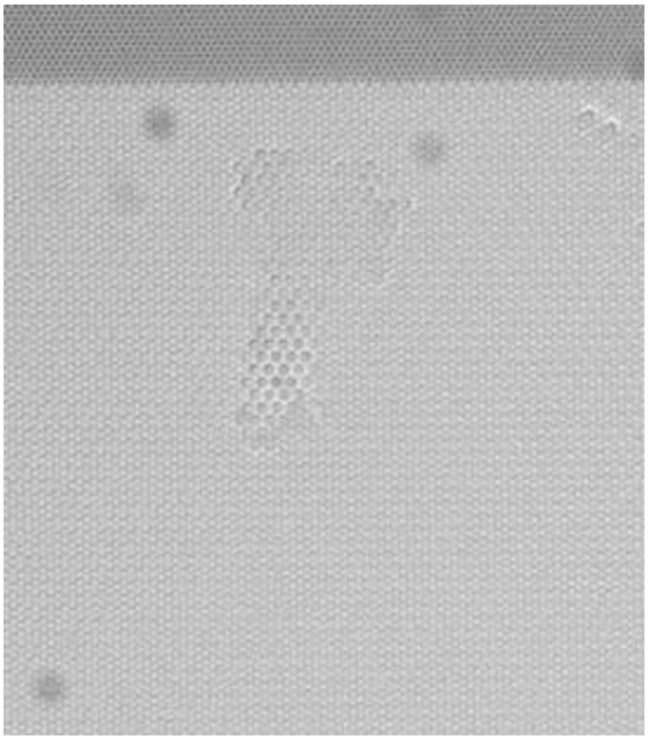

Movie S3. An example of the cell movements at the boundary between a stiff substrate ($K = 80$ nN/μm; pillar diameter $= 2$ μm) and a soft substrate ($k = 7$ nN/μm; pillar diameter $= 1$ μm). The cell is coming from the stiff part of the substrate, probes the soft part, rotates, but stays on the stiff side.
Movie S3 (MOV)

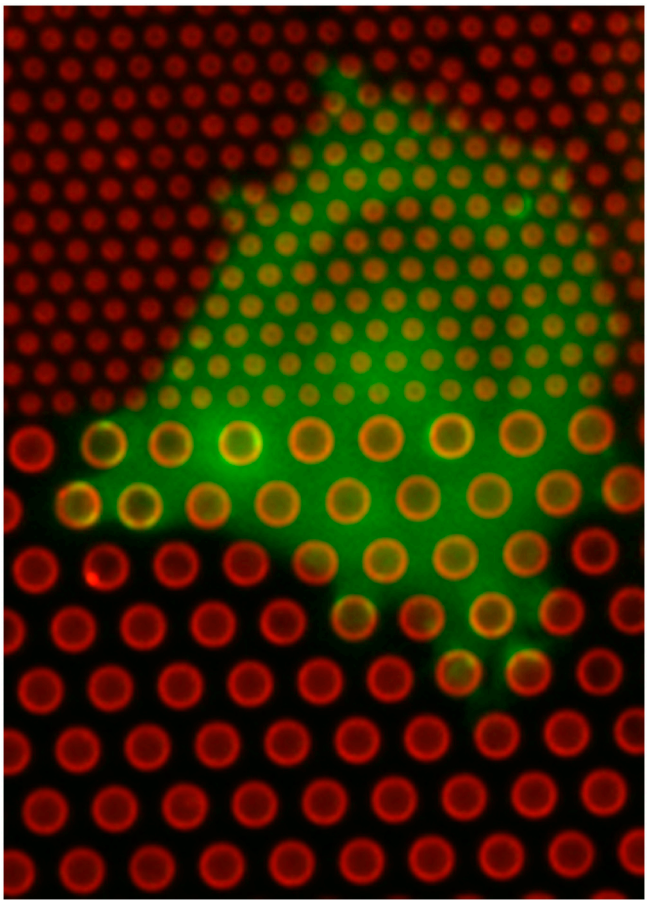

Movie S4. Local deformations of the substrate at the interface between soft and stiff parts. Pillars are in red and cell staining in green. The transmigration process toward the stiff part induces a sudden increase of the force normal to the boundary.
Movie S4 (MOV)